ACS OMEGA

Open Access

http://pubs.acs.org/journal/acsodf

Article

Cobalt Hydroxide Modification of TiO_2 Nanosheets for Visible-Light-Responsive Photocatalysts

Hidehisa Hagiwara,* Katsuaki Hayakawa, Kazuki Ishitsuka, Keisuke Awaya, Kazuto Hatakeyama, and Shintaro Ida

Cite This: *ACS Omega* 2025, 10, 3101−3107

Read Online

ACCESS | Metrics & More | Article Recommendations | Supporting Information

ABSTRACT: To make full use of sunlight for water splitting reactions for hydrogen production, a visible-light-driven photocatalyst was developed by modifying TiO_2 nanosheets with $Co(OH)_2$. By adding an aqueous $Co(NO_3)_2{\cdot}6H_2O$ solution to a TiO_2 nanosheet suspension, the TiO_2 nanosheets aggregated and $Co(OH)_2$ was formed. In the ultraviolet−visible (UV−vis) diffuse reflectance spectrum of the photocatalyst, new absorption bands attributable to $Co(OH)_2$ and the interfacial charge transfer between $Co(OH)_2$ and the TiO_2 nanosheets appeared at around 600 and 400 nm, respectively. The photocatalytic activity of $Co(OH)_2/TiO_2$ nanosheets was evaluated in terms of the O_2 evolution reaction in an aqueous $AgNO_3$ solution, finding that the reaction proceeds under visible light. Furthermore, the investigation of the wavelength dependence of the photocatalytic activity revealed that the photocatalytic reaction on $Co(OH)_2/TiO_2$ nanosheets proceeds via $Co(OH)_2$ photocatalysis and interfacial charge transfer between $Co(OH)_2$ and the TiO_2 nanosheets under visible light irradiation.

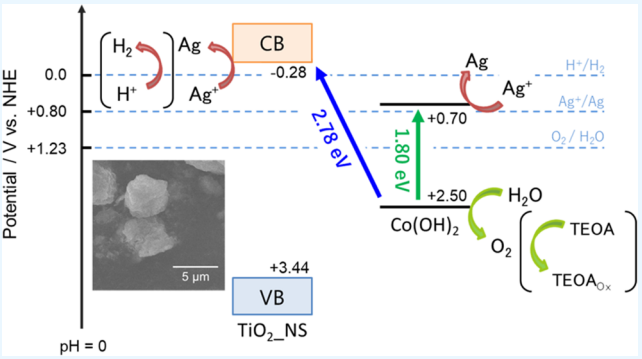

1. INTRODUCTION

To achieve carbon neutrality, making full use of renewable energy sources has recently become a hot research field. In this context, photocatalytic water splitting for hydrogen production using solar energy stands out as a promising process,[1−3] for which wide bandgap semiconductor oxides such as Al-doped $SrTiO_3$, La-doped $NaTaO_3$, and Ga_2O_3 have been reported as photocatalysts with high quantum yields.[4−9] However, since the proportion of ultraviolet (UV) light in sunlight is small, developing photocatalysts for water splitting that can utilize visible and infrared light, which comprise a large portion of sunlight, is highly desirable.

To develop highly efficient photocatalysts, it is important to synthesize materials with large surface area and high crystallinity and to separate oxidation and reduction sites to prevent charge recombination and backward reactions.[10,11] Oxide nanosheets, which are two-dimensional (2D) anisotropic semiconductor materials with a thickness of a few nanometers and a lateral direction of a few micrometers, possess relatively high crystallinity and high surface area. Moreover, oxide nanosheets feature advantages such as separation of reaction sites, suppression of recombination due to the short migration distance to the surface, and ability to harvest more photons than nanoparticles, which render them promising candidates as water splitting photocatalysts.[12] However, most oxide nanosheets, such as TiO_2[13,14] $HTiNbO_5$,[15,16] and $Ca_2Nb_3O_{10}$,[17] have a large bandgap and cannot utilize visible light directly.

To utilize visible light energy, various approaches have been adopted to develop visible-light-responsive photocatalysts, such as bandgap narrowing by cation or anion doping[18,19] and dye sensitization via organic dye modification on the semiconductor surface.[20,21] Hydrogen production reactions and dye degradation under visible light using composite photocatalysts composed of TiO_2 and nanosheets,[22,23] nanotubes,[24,25] or nanorods[26,27] have been reported. The development of visible-light-responsive photocatalysts by loading metal compound nanoclusters on wide bandgap oxide semiconductors has also been reported.[28,29] In previous studies, Hashimoto et al. studied the visible-light oxidation of 2-propanol by loading nanoparticles of metal species such as Cu,[30] Cr,[31] and Rh[32] onto TiO_2 or WO_3. Furthermore, a photoelectrochemical cell system consisting of a $Co(OH)_2$ nanoparticle/TiO_2/FTO electrode was applied for the water oxidation reaction.[33] This system relies in the transfer of

Received: November 7, 2024
Revised: January 2, 2025
Accepted: January 8, 2025
Published: January 16, 2025

https://doi.org/10.1021/acsomega.4c10161
ACS Omega 2025, 10, 3101−3107

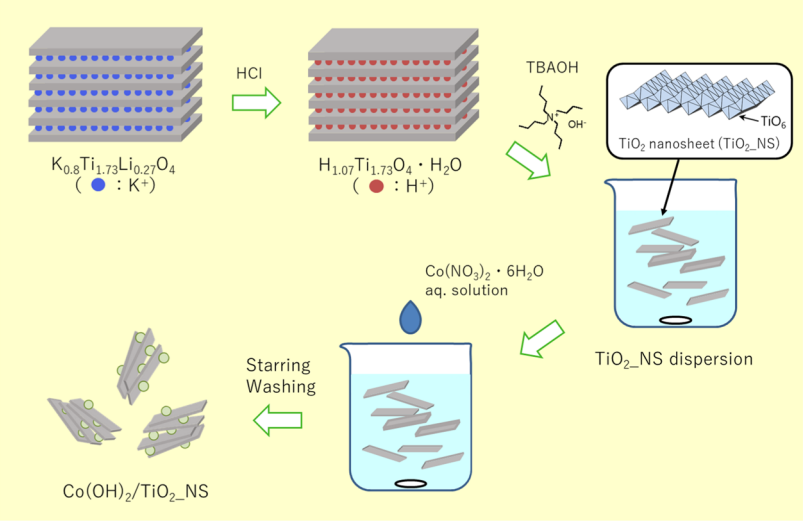

Figure 1. Preparation procedure for the $Co(OH)_2/TiO_2$_NS photocatalyst.

electrons from Co nanoparticles to the conduction band of the metal oxide and subsequent oxidation of water by the electron-deficient Co species. Thus, the supported Co species play two roles: promoting the electron transfer to the metal oxide and water oxidation. In addition, the study of the wavelength dependence of photocatalytic activity showed a correlation with light absorption in the visible light range. Therefore, surface modification using metal nanoparticles is an effective approach to prepare visible-light-responsive photocatalysts. Herein, a photocatalyst was prepared by loading Co species onto TiO_2 nanosheets (TiO_2_NS) to utilize visible light energy for photocatalytic reactions. The photocatalytic activity of the Co-modified TiO_2_NS photocatalyst was evaluated in the O_2 evolution reaction in an aqueous $AgNO_3$ solution. Furthermore, the charge-transfer mechanism of the photocatalysts was investigated on the basis of the wavelength dependence of the photocatalytic activity. Unlike the case of Co-modified bulk TiO_2 powder, the oxygen evolution reaction proceeded by multiple reaction mechanisms in Co-modified TiO_2_NS.

2. EXPERIMENTAL SECTION

2.1. Photocatalyst Preparation. The preparation process of the $Co(OH)_2/TiO_2$_NS photocatalyst is shown in Figure 1. All reagents were used as received without further purification. TiO_2_NS was prepared as previously reported.[14] First, layered oxide $K_{0.8}Ti_{1.73}Li_{0.27}O_4$ was synthesized using a solid-state reaction method as follows: K_2CO_3 (99.5%, FUJIFILM Wako Pure Chemical Corp.), $LiCO_3$ (99.0%, FUJIFILM Wako Pure Chemical Corp.), and TiO_2 (99%, Kojundo Chemical Laboratory) with a molar ratio of 0.8:1.73:0.27 were ground in an alumina mortar. The obtained mixture was precalcined at 1073 K for 30 min in air and then ground and calcined at 1073 K for 20 h in air. The as-synthesized $K_{0.8}Ti_{1.73}Li_{0.27}O_4$ was added to 1 M HCl for 1 week to exchange K^+ and Li^+ for H^+. The proton-exchanged compound was exfoliated by immersing it in a 25 mM aqueous tetrabutylammonium hydroxide (TBAOH) solution to obtain TiO_2_NS. The yield of TiO_2_NS prepared from the proton-exchanged compound was about 47%. The low yield of TiO_2 nanosheet is attributed to the incomplete exfoliation of the proton-exchanged compound. $Co(OH)_2$ modification of TiO_2_NS was performed by mixing an aqueous $Co(NO_3)_2 \cdot 6H_2O$ (99.5%, FUJIFILM Wako Pure Chemical Corp., 1−20 wt % relative to TiO_2_NS) solution and a TiO_2_NS suspension. After stirring at 200 rpm for 1 h, two washing cycles, and vacuum drying, the $Co(OH)_2/TiO_2$_NS photocatalyst was obtained. The yield of the catalyst after Co modification was about 45%. The low yield of Co-modified TiO_2 nanosheets is due to the strong adsorption of TiO_2 nanosheets on the beaker surface during preparation.

2.2. Characterization. The crystal structure was examined via powder X-ray diffraction (XRD; X' Pert MPD, PANalytical) with Cu Kα radiation (1.541 Å) using a tube voltage of 45 kV and a tube current of 40 mA. The sample morphology was determined via field emission scanning electron microscopy (FE-SEM; JEOL, JSM-6701F) combined with energy dispersive X-ray spectroscopy (EDX; JEOL, JED-2300). X-ray photoelectron spectroscopy (XPS; Thermo Fisher Scientific, ESCALAB250Xi) and Fourier transform infrared spectroscopy (FT-IR; Jasco, FT/IR-4600) were used to identify the Co species. Diffuse reflectance spectra were measured using a ultraviolet−visible (UV−vis) spectrophotometer (Jasco, ISV-469). The reflectance was converted to absorbance using the Kubelka−Munk function with $BaSO_4$ as the baseline.

2.3. Photocatalytic Reaction. The photocatalytic reaction was performed in a glass closed-circulation reactor. The photocatalyst (20 mg) was dispersed in a quartz cell containing 10 mM $AgNO_3$ (FUJIFILM Wako Pure Chemical Corp.) aqueous solution or 250 mM triethanolamine (TEOA, 98.0%, FUJIFILM Wako Pure Chemical Corp.) aqueous solution (30 mL). When triethanolamine was used as a sacrificial agent, $H_2PtCl_6 \cdot 6H_2O$ (98.5%, FUJIFILM Wako Pure Chemical Corp.) was added as a Pt cocatalyst precursor (0.2 wt %). The reaction cell was irradiated using a 300 W Xe lamp (350 nm < λ < 800 nm; Asahi Spectra Co., Ltd.) under magnetic stirring. The evolved gases were detected using a gas chromatograph with a thermal conductivity detector. Apparent quantum yields (AQYs) for O_2 evolution reaction were measured using the 300 W Xe lamp with a bandpass filter (λ: 430, 470, 520, 570, 620, 660, and 720 nm). The AQY values were calculated by using the following equation:

https://doi.org/10.1021/acsomega.4c10161
ACS Omega 2025, 10, 3101−3107

$$\mathrm{AQY}(\%) = (A \times N)/(I \times t) \times 100 \quad (1)$$

where A, N, I, and t represent the coefficient of O_2 formation ($A = 4$), the amount of formed O_2, the number of incident photons, and the reaction time, respectively. The total number of incident photons was measured using an optical power meter (Newport Corp., 1936-R) with a thermopile sensor (Newport Corp., 919P-010−16).

3. RESULTS AND DISCUSSION

3.1. Characterization of the Co-Modified TiO_2_NS Photocatalyst. The preparation procedure for $Co(OH)_2$/TiO_2_NS is shown in Figure 1. The layered oxide $K_{0.8}Ti_{1.73}Li_{0.27}O_4$ was used as the starting material for TiO_2_NS. XRD measurements confirmed that a lepidocrocite-type layered oxide with K^+ between the layers of an edge-shared octahedral corrugated host layer was obtained (Figure S1). The XRD patterns of the proton-exchanged compound and TiO_2_NS are also shown in Figure S1. The diffraction peaks of TiO_2_NS can be attributed to the TiO_2 nanosheets, as previously reported.[14] The size of the obtained TiO_2_NS was determined to be a few micrometers in the vertical direction and approximately 1.2 nm in thickness from the atomic force microscopy image (Figure S2). The obtained nanosheets were thicker than the theoretical thickness (0.75 nm), presumably due to the adsorption of water or TBA on the nanosheet surface. Figure 2 shows XRD patterns of TiO_2_NS loaded with

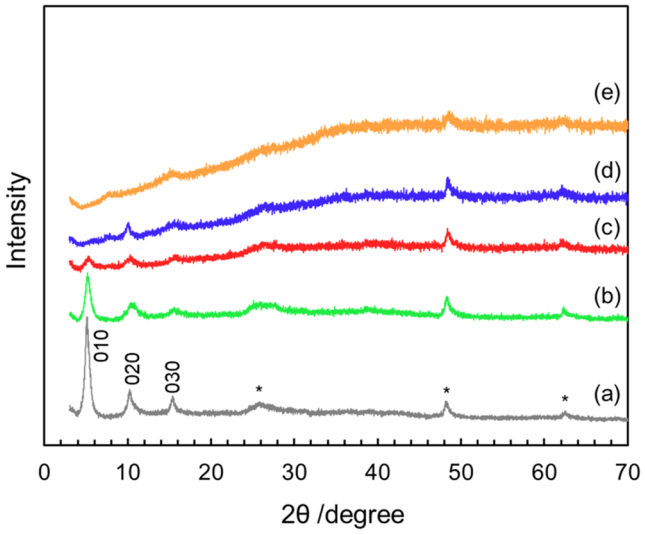

Figure 2. XRD patterns of (a) TiO_2_NS and TiO_2_NS loaded with (b) 1 wt %, (c) 5 wt %, (d) 10 wt %, and (e) 20 wt % $Co(OH)_2$.

different amounts of $Co(OH)_2$. The diffraction peaks at 5.2, 10.4, and 15.6° were attributed to regularly stacked TiO_2_NS and around 26, 48, and 62° are probably due to fine particles of $K_{0.8}Ti_{1.73}Li_{0.27}O_4$ or $H_{1.07}Ti_{1.73}O_4$, which are precursors of TiO_2 nanosheets. The diffraction peaks of Co species were not observed. The diffraction peak intensity of the (010) plane decreased considerably with increasing Co loading amount. This result suggests that the nanosheets in TiO_2_NS were randomly stacked due to Co loading, and the *b*-axis-oriented TiO_2_NS became disordered. Brunauer−Emmett−Teller (BET) specific surface area measurements showed that the surface areas of TiO_2_NS aggregates and $Co(OH)_2$/TiO_2_NS were 42.8 and 34.5, respectively. It is suggested that the Co loading caused TiO_2_NS stacking, which reduced the surface area. To confirm the morphology of the catalyst, SEM−EDX observations were performed. Figure 3a shows the SEM image of $Co(OH)_2$/TiO_2_NS, in which stacked and aggregated nanosheets can be observed. Figure 3b−d show the EDX mapping images of $Co(OH)_2$ (10 wt %)/TiO_2_NS. Co species were highly dispersed in the TiO_2_NS aggregates, which explains why XRD peaks from Co species were not observed.

To identify the oxidation states of the Co species, XPS measurements were performed. Figure 4 shows the XPS spectra of Co-loaded TiO_2_NS, in which two main peaks at 780.6 and 796.6 eV were observed along with satellite peaks at 787.1 and 803.6 eV, suggesting the presence of divalent Co species.[34−36]

Figure 5a,5b shows the FT-IR spectra of Co-loaded TiO_2_NS. The peaks at 2800−3000 and 1650 cm^{-1} were attributed to the C−H stretching vibration and the C−H bending vibration of TBAOH, respectively. It suggests that the prepared photocatalysts contain TBAOH. These results were also suggested by the regularly stacked structure observed in the XRD pattern (Figure 2), which correlates in good agreement with the decrease with increasing $Co(OH)_2$ loading amount. For all catalysts, including TiO_2_NS, a broad absorption at 3000−3650 cm^{-1} attributable to surface-adsorbed water was observed. Figure 5c shows the differential spectra of Co-loaded TiO_2_NS and TiO_2_NS. Relatively sharp peaks attributed to the stretching vibration of the OH group appeared around 3600 cm^{-1}. Such a peak was also observed in the FT-IR spectrum of $Co(OH)_2$ (Figure 5b), which together with the XPS results indicates that the Co species loaded on TiO_2_NS was $Co(OH)_2$.

Figure 6 shows the UV−vis diffuse reflectance spectra of $Co(OH)_2$/TiO_2_NS. New absorption bands appeared in the visible light region, and the intensity of light absorption increased with increasing $Co(OH)_2$ loading. According to a previous report, the absorption near 600 nm was assigned to $Co(OH)_2$.[37] $Co(OH)_2$ is formed as a layered compound on 2D compounds such as rGO and LDH.[38,39] Therefore, $Co(OH)_2$ on TiO_2_NS might also be formed as a layered compound. Meanwhile, the absorption at around 400 nm is most likely due to interfacial charge transfer between $Co(OH)_2$ and TiO_2_NS.

3.2. Photocatalytic Activity Evaluation. The photocatalytic activity was evaluated using the O_2 evolution reaction as a model reaction in an aqueous solution of $AgNO_3$ as a sacrificial reagent. In this reaction, Ag^+ acts as a scavenger of electrons photogenerated in the photocatalyst, and the remaining holes oxidize water to produce O_2, as shown in the following equations:

$$\text{reduction reaction:} \quad Ag^+ + e^- \rightarrow Ag \quad (2)$$

$$\text{oxidation reaction:} \quad 2H_2O \rightarrow O_2 + 4H^+ + 4e^- \quad (3)$$

The O_2 evolution activity of TiO_2_NS modified with various transition metal hydroxides was evaluated (Figure S3). Because the highest activity was observed for the catalyst loaded with Co species, the modification effect of Co species was investigated in detail. Previous studies using bulk TiO_2 have also reported that cobalt is highly effective as the modification material.[28] This is because the photocatalytic performance is affected by the oxidation ability of the modification materials. In the case of $Co(OH)_2$/TiO_2_NS photocatalyst, the pH value of the reaction solution was changed from 6.5 to 3.8 after 3h of

https://doi.org/10.1021/acsomega.4c10161
ACS Omega 2025, 10, 3101−3107

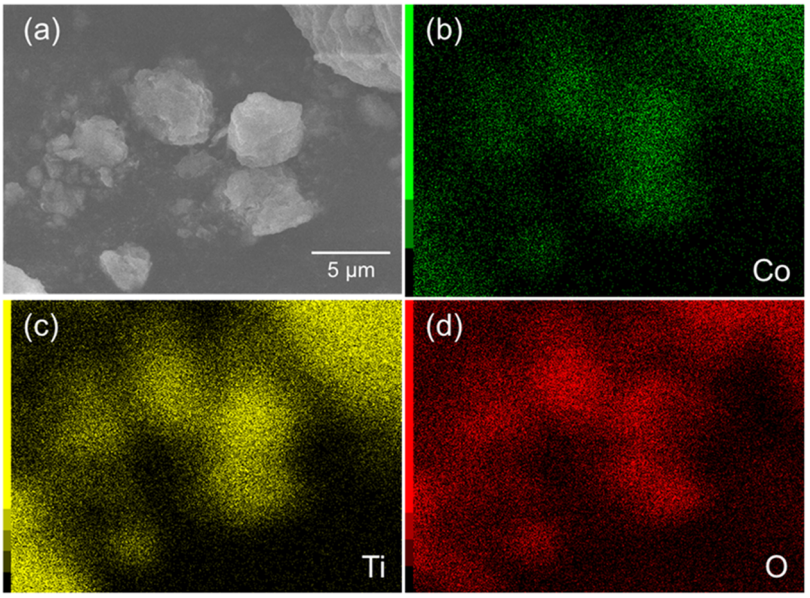

Figure 3. (a) SEM image and (b) Co, (c) Ti, and (d) O EDX mapping images of $Co(OH)_2$ (10 wt %)/TiO_2_NS.

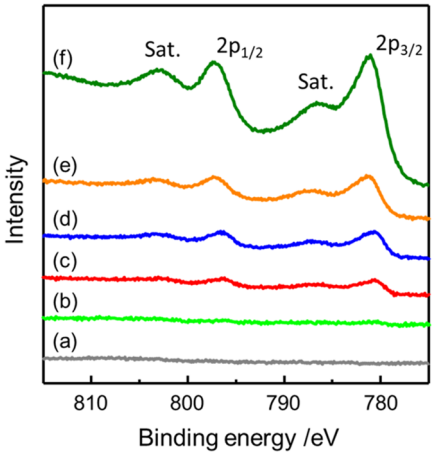

Figure 4. XPS spectra of (a) TiO_2_NS, TiO_2_NS loaded with (b) 1 wt %, (c) 5 wt %, (d) 10 wt %, and (e) 20 wt % $Co(OH)_2$, and (f) $Co(OH)_2$.

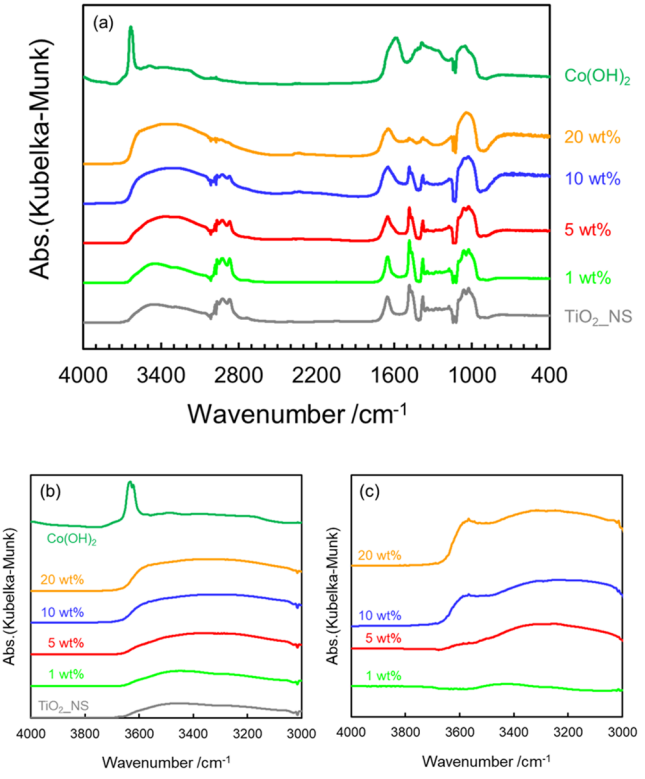

Figure 5. (a) FT-IR spectra of TiO_2_NS, $Co(OH)_2$/TiO_2_NS, and $Co(OH)_2$. (b) Expand image of FT-IR spectra. (c) Differential FT-IR spectra of $Co(OH)_2$/TiO_2_NS and TiO_2_NS.

light irradiation, suggesting that H^+ is formed simultaneously with the formation of O_2 gas, as shown in eq 3. After the reaction, the $Co(OH)_2$/TiO_2_NS photocatalyst was analyzed by XRD, XPS, and STEM-EDS (Figures S4–S6). The results showed that the metal Ag was deposited on the catalyst. To confirm that the oxygen evolved photocatalytically, a long-term reaction for O_2 evolution from 50 mM $AgNO_3$ aqueous solution at 283 K under Xe lamp irradiation (1.25 W cm^{-2}, 350 nm < λ < 800 nm). The photocatalytic reaction was repeated for 5 cycles, with the reactor evacuated every 96 h (Figure S7a). Although the O_2 formation rate gradually decreased due to the Ag deposition, the O_2 formation amount reached 288 μmol in 480 h (Figure S7b). The photocatalyst is 20 mg $Co(OH)_2$ (10 wt %)/TiO_2_NS, with moles of 250 μmol (TiO_2_NS) and 21.5 μmol ($Co(OH)_2$), respectively. It was confirmed that the photocatalyst was able to produce O_2 with turnover numbers (TON) > 1, thus the oxygen evolved by the photocatalytic reaction.

Figure 7a shows the relationship between the loading amount of $Co(OH)_2$ and the rate of O_2 evolution in a $AgNO_3$ solution under visible light illumination (350 nm < λ < 800 nm). All catalysts showed photocatalytic activity, with $Co(OH)_2$ (10 wt %)/TiO_2_NS exhibiting the highest O_2 evolution rate (0.38 μmol/h). It is suggested that the improvement of O_2 evolution activity is due to the increase in visible light absorption with increasing $Co(OH)_2$ loading. On the other hand, the O_2 evolution rate decreased with an excess amount of $Co(OH)_2$ loading. Therefore, in addition to the light absorption of the catalyst, the improvement of O_2

https://doi.org/10.1021/acsomega.4c10161
ACS Omega 2025, 10, 3101−3107

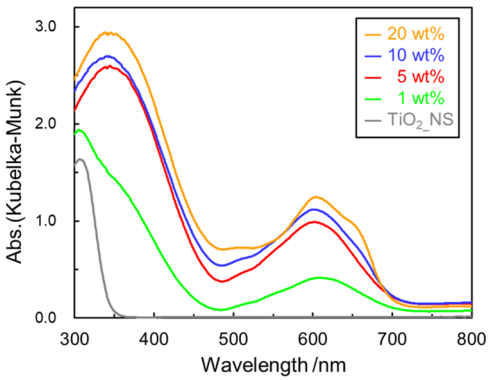

Figure 6. UV−vis diffuse reflectance spectra of $Co(OH)_2/TiO_2$_NS and TiO_2_NS.

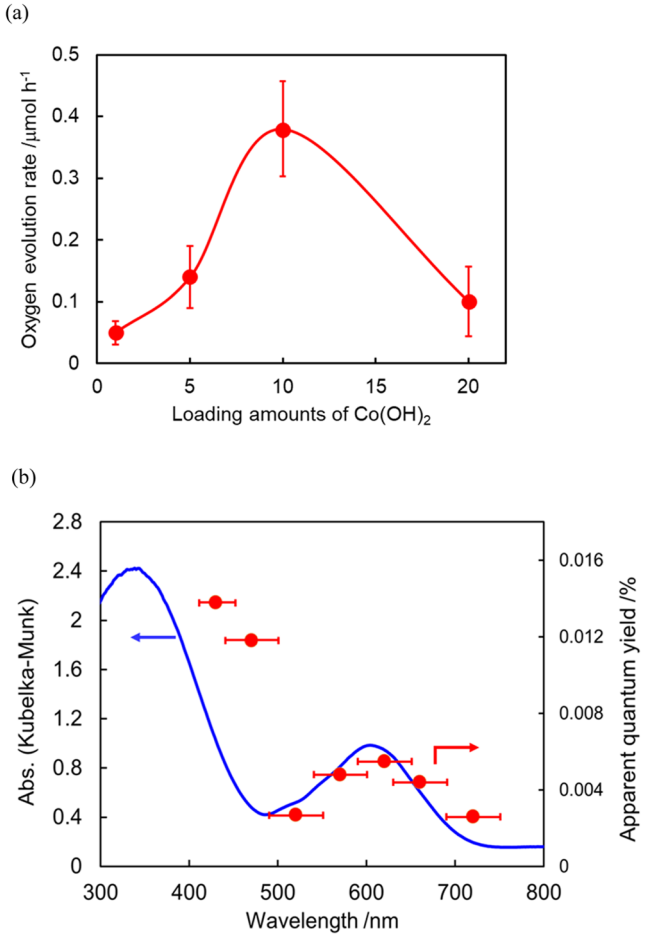

Figure 7. (a) O_2 evolution rates on $Co(OH)_2/TiO_2$_NS in a 10 mM $AgNO_3$ aqueous solution under Xe lamp irradiation (0.57 W cm^{-2}, 350 nm < λ < 800 nm). (b) Relationship between the apparent quantum yield of $Co(OH)_2$ (10 wt %)/TiO_2_NS on O_2 evolution reaction and UV−vis diffuse reflectance spectrum of the photocatalyst.

evolution activity should be considered the influence of TiO_2_NS adsorption on the carrier mobility of $Co(OH)_2$ and the coating effect of TiO_2_NS on $Co(OH)_2$.[40] Figure 7b shows the apparent quantum yields of O_2 evolution reaction on $Co(OH)_2$ (10 wt %)/TiO_2_NS under irradiation with a Xe lamp with a bandpass filter (430, 470, 520, 570, 620, 660, and 720 nm). The error bars indicate the wavelength range of transmitted light through the band-pass filter. It was found that the apparent quantum yield was in good agreement with the absorption spectrum of $Co(OH)_2$ (10 wt %)/TiO_2_NS. This result indicates that the O_2 evolution reaction under visible light irradiation proceeds upon loading $Co(OH)_2$ onto TiO_2_NS, which otherwise would only absorb UV light. As mentioned above, the optical absorptions at around 600 and 400 nm can be attributed to $Co(OH)_2$ and the interfacial charge transfer transition, respectively, indicating that both features contribute to the O_2 evolution reaction on $Co(OH)_2/TiO_2$_NS. This result is specific to the Co modification of TiO_2 nanosheets, as it has not been reported for Co-modified TiO_2 powder photocatalysts.[33] This is presumed to be due to the formation of α-$Co(OH)_2$, a two-dimensional material that exhibits photocatalytic activity, on the surface of the TiO_2 nanosheets.[37] If multiple photoexcitation mechanisms can be constructed within a photocatalyst, it could be applied to the design of highly efficient photocatalysts under sunlight irradiation.

To identify the interfacial charge transfer transition from $Co(OH)_2$ to TiO_2_NS, the hydrogen evolution reaction was investigated using a triethanolamine solution as a sacrificial reagent. In this experiment, a Pt catalyst was loaded on $Co(OH)_2/TiO_2$_NS via the photodeposition method. The photocatalytic activity of $Pt/Co(OH)_2/TiO_2$_NS was evaluated using a 300 W Xe lamp with bandpass filters of 630 and 430 nm. As shown in Figure 8, no hydrogen was observed

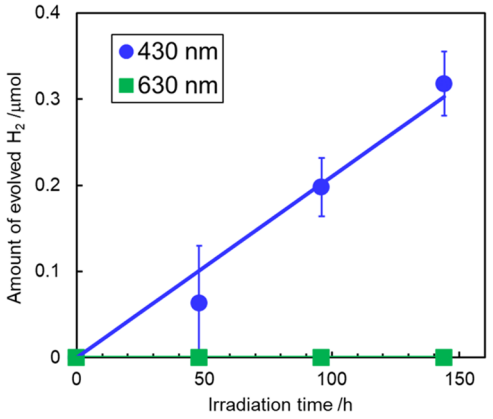

Figure 8. Time course of H_2 evolution on $Pt/Co(OH)_2/TiO_2$_NS in a 0.25 M triethanolamine aqueous solution under illumination of Xe lamp with a bandpass filter.

under 630 nm light irradiation, whereas hydrogen evolution was observed under 430 nm light irradiation. The results indicate that an interface charge transition occurs from $Co(OH)_2$ to TiO_2_NS, according to which the charge transfer mechanism depicted in Figure 9 can be proposed for the $Co(OH)_2/TiO_2$_NS photocatalyst. The energy levels for TiO_2_NS and $Co(OH)_2$ were drawn according to the estimated bandgap value (Figures S8 and S9) and the literature.[13,39] The conduction bands of TiO_2_NS and $Co(OH)_2$ have sufficient potential to allow the Ag^+ reduction reaction to proceed. In addition, the holes generated in the valence band of $Co(OH)_2$ have sufficient potential to oxidize water to produce O_2. Meanwhile, the potential of the conduction band of $Co(OH)_2$ is not enough to promote the hydrogen evolution reaction, whereas that of TiO_2_NS is sufficient. Thus, not only the interface charge transition from

https://doi.org/10.1021/acsomega.4c10161
ACS Omega 2025, 10, 3101−3107

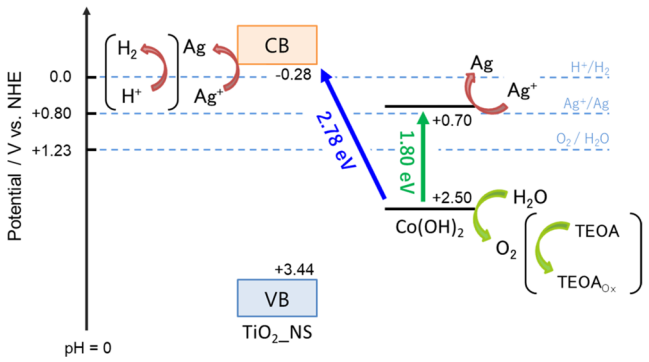

Figure 9. Proposed charge-transfer mechanism in the $Co(OH)_2$/TiO_2_NS photocatalyst.

$Co(OH)_2$ to TiO_2_NS but also the $Co(OH)_2$ photocatalysis contribute to the photocatalytic reaction of $Co(OH)_2$/TiO_2_NS.

4. CONCLUSIONS

In this study, the effect of Co loading on the visible light responsivity of TiO_2_NS photocatalysts was investigated. The $Co(OH)_2$/TiO_2_NS stacked photocatalyst was prepared by adding $Co(NO_3)_2 \cdot 6H_2O$ to a suspension of TiO_2_NS exfoliated from $K_{0.8}Ti_{1.73}Li_{0.27}O_4$. In the UV−vis diffuse reflectance spectra, new absorption bands appeared in the visible light region upon loading Co species onto TiO_2_NS, i.e., an absorption at approximately 600 nm ascribable to $Co(OH)_2$ and another near 400 nm due to the interfacial charge transfer between $Co(OH)_2$ and TiO_2_NS. The photocatalytic activity of TiO_2_NS with different amounts of $Co(OH)_2$ loading was investigated in the O_2 evolution reaction in aqueous $AgNO_3$ solution. O_2 evolution activity under visible light was observed for all the examined $Co(OH)_2$/TiO_2_NS catalysts, among which the catalyst with 10 wt % $Co(OH)_2$ loading exhibited the highest activity. The wavelength dependence of the photocatalytic activity of $Co(OH)_2$/TiO_2_NS revealed that the photocatalytic reaction is promoted by $Co(OH)_2$ photocatalysis and the interfacial charge transfer between $Co(OH)_2$ and TiO_2_NS under visible light irradiation. The results obtained in this study can be applied to a photocatalyst design for solar water splitting and are expected to contribute to the development of visible-light-responsive photocatalysts using 2D materials such as TiO_2 nanosheets.

■ ASSOCIATED CONTENT

Supporting Information

The Supporting Information is available free of charge at https://pubs.acs.org/doi/10.1021/acsomega.4c10161.

Powder XRD, AFM image, photocatalytic OER, post XRD, XPS; HAADF-STEM images and EDS spectrum; long-term photocatalytic activity evaluation; UV−vis DR spectrum and Tauc plots for bandgap calculation (PDF)

■ AUTHOR INFORMATION

Corresponding Author

Hidehisa Hagiwara − *Hydrogen Isotope Research Center, Organization for Promotion of Research, University of Toyama, Toyama 930-8555, Japan;* orcid.org/0000-0002-6557-0923; Phone: +81-76-445-6932; Email: hhagi@ctg.u-toyama.ac.jp

Authors

Katsuaki Hayakawa − *Hydrogen Isotope Research Center, Organization for Promotion of Research, University of Toyama, Toyama 930-8555, Japan*

Kazuki Ishitsuka − *Hydrogen Isotope Research Center, Organization for Promotion of Research, University of Toyama, Toyama 930-8555, Japan*

Keisuke Awaya − *Faculty of Advanced Science and Technology, Kumamoto University, Kumamoto 860-8555, Japan;* orcid.org/0000-0002-4482-2693

Kazuto Hatakeyama − *Institute of Industrial Nanomaterials (IINa), Kumamoto University, Kumamoto 860-8555, Japan*

Shintaro Ida − *Institute of Industrial Nanomaterials (IINa), Kumamoto University, Kumamoto 860-8555, Japan;* orcid.org/0000-0002-0032-1897

Complete contact information is available at: https://pubs.acs.org/10.1021/acsomega.4c10161

Notes

The authors declare no competing financial interest.

■ ACKNOWLEDGMENTS

This research was supported by a JSPS KAKENHI Grant-in-Aid for Scientific Research (C) (23K04908).

■ REFERENCES

(1) Segev, G.; Kibsgaard, J.; Hahn, C.; Xu, Z. J.; Cheng, W.-H.; Deutsch, T. G.; Xiang, C.; Zhang, J. Z.; Hammarström, L.; Nocera, D. G.; et al. The 2022 Solar Fuels Roadmap. *J. Phys. D: Appl. Phys.* **2020**, *55*, No. 323003.

(2) Chen, X. B.; Shen, S. H.; Guo, L. J.; Mao, S. S. Semiconductor-based Photocatalytic Hydrogen Generation. *Chem. Rev.* **2010**, *110*, 6503−6570.

(3) Pinaud, B. A.; Benck, J. D.; Seitz, L. C.; Forman, A. J.; Chen, Z. B.; Deutsch, T. G.; James, B. D.; Baum, K. N.; Baum, G. N.; Ardo, S.; Wang, H. L.; Miller, E.; Jaramillo, T. F. Technical and Economic Feasibility of Centralized Facilities for Solar Hydrogen Production via Photocatalysis and Photoelectrochemistry. *Energy Environ. Sci.* **2013**, *6*, 1983−2002.

(4) Takata, T.; Jiang, J.; Sakata, Y.; Nakabayashi, M.; Shibata, N.; Nandal, V.; Seki, K.; Hisatomi, T.; Domen, K. Photocatalytic Water Splitting with a Quantum Efficiency of Almost Unity. *Nature* **2020**, *581*, 411−414.

(5) Lyu, H.; Hisatomi, T.; Goto, Y.; Yoshida, M.; Higashi, T.; Katayama, M.; Takata, T.; Minegishi, T.; Nishiyama, H.; Yamada, T.; Sakata, Y.; Asakura, K.; Domen, K. An Al-doped $SrTiO_3$ Photocatalyst Maintaining Sunlight-driven Overall Water Splitting Activity for over 1000 h of Constant Illumination. *Chem. Sci.* **2019**, *10*, 3196−3201.

(6) Kato, H.; Asakura, K.; Kudo, A. Highly Efficient Water Splitting into H_2 and O_2 over Lanthanum-doped $NaTaO_3$ Photocatalysts with High Crystallinity and Surface Nanostructure. *J. Am. Chem. Soc.* **2003**, *125*, 3082−3089.

(7) Kato, H.; Kudo, A. Water Splitting into H_2 and O_2 on Alkali Tantalate Photocatalysts $ATaO_3$ (A = Li, Na, and K). *J. Phys. Chem. B* **2001**, *105*, 4285−4292.

(8) Kudo, A.; Kato, H. Effect of Lanthanide-doping into $NaTaO_3$ Photocatalysts for Efficient Water Splitting. *Chem. Phys. Lett.* **2000**, *331*, 373−377.

(9) Sakata, Y.; Hayashi, T.; Yasunaga, R.; Yanaga, N.; Imamura, H. Remarkably High Apparent Quantum Yield of the Overall Photocatalytic H_2O Splitting Achieved by Utilizing Zn Ion Added Ga_2O_3 Prepared Using Dilute $CaCl_2$ Solution. *Chem. Commun.* **2015**, *51*, 12935−12938.

(10) Liu, Y.; Wu, H.; Wang, Q. Strategies to Improve the Photocatalytic Performance of Covalent Triazine Frameworks. *J. Mater. Chem. A* **2023**, *11*, 21470−21497.
(11) Yang, L.; Yu, J.; Fu, Q.; Kong, L.; Xu, X. Mesoporous Single-crystalline $SrNbO_2N$: Expediting Charge Transportation to Advance Solar Water Splitting. *Nano Energy* **2022**, *95*, No. 107059.
(12) Ida, S.; Ishihara, T. Recent Progress in Two-Dimensional Oxide Photocatalysts for Water Splitting. *J. Phys. Chem. Lett.* **2014**, *5* (15), 2533−2542.
(13) Sakai, N.; Kamanaka, K.; Sasaki, T. Modulation of Photochemical Activity of Titania Nanosheets via Heteroassembly with Reduced Graphene Oxide. Enhancement of Photoinduced Hydrophilic Conversion Properties. *J. Phys. Chem. C* **2016**, *120* (42), 23944−23950.
(14) Maluangnont, T.; Matsuba, K.; Geng, F.; Ma, R.; Yamauchi, Y.; Sasaki, T. Osmotic Swelling of Layered Compounds as a Route to Producing High-Quality Two-Dimensional Materials. A Comparative Study of Tetramethylammonium versus Tetrabutylammonium Cation in a Lepidocrocite-type Titanate. *Chem. Mater.* **2013**, *25* (15), 3137−3146.
(15) Lin, H.-Y.; Chang, Y.-S. Photocatalytic Water Splitting on Au/$HTiNbO_5$ Nanosheets. *Int. J. Hydrogen Energy* **2014**, *39*, 3118−3126.
(16) Du, G. H.; Yu, Y.; Chen, Q.; Wang, R. H.; Zhou, W.; Peng, L.-M. Exfoliating $KTiNbO_5$ Particles into Nanosheets. *Chem. Phys. Lett.* **2003**, *377*, 445−448.
(17) Okamoto, Y.; Ida, S.; Hyodo, J.; Hagiwara, H.; Ishihara, T. Synthesis and Photocatalytic Activity of Rhodium-Doped Calcium Niobate Nanosheets for Hydrogen Production from a Water/Methanol System without Cocatalyst Loading. *J. Am. Chem. Soc.* **2011**, *133*, 18034−18037.
(18) Ida, S.; Okamoto, Y.; Matsuka, M.; Hagiwara, H.; Ishihara, T. Preparation of Tantalum-Based Oxynitride Nanosheets by Exfoliation of a Layered Oxynitride, $CsCa_2Ta_3O_{10-x}N_y$, and Their Photocatalytic Activity. *J. Am. Chem. Soc.* **2012**, *134* (38), 15773−15782.
(19) Asahi, R.; Morikawa, T.; Ohwaki, T.; Aoki, K.; Taga, Y. Visible-light Photocatalysis in Nitrogen-doped Titanium Oxides. *Science* **2001**, *293*, 269−271.
(20) Park, H.; Choi, W. Visible-Light-Sensitized Production of Hydrogen Using Perfluorosulfonate Polymer-Coated TiO_2 Nanoparticles: An Alternative Approach to Sensitizer Anchoring. *Langmuir* **2006**, *22* (6), 2906−2911.
(21) Kalyanasundaram, K.; Vlachopoulos, N.; Krishnan, V.; Monnier, A.; Grätzel, M. Sensitization of Titanium Dioxide in the Visible Light Region Using Zinc Porphyrins. *J. Phys. Chem. A* **1987**, *91* (9), 2342−2347.
(22) Qiu, B.; Zhou, Y.; Ma, Y.; Yang, X.; Sheng, W.; Xing, M.; Zhang, J. Facile Synthesis of the Ti^{3+} Self-doped TiO_2-Graphene Nanosheet Composites with Enhanced Photocatalysis. *Sci. Rep.* **2015**, *5*, No. 8591.
(23) Chen, L.; Ye, X.; Chen, S.; Ma, L.; Wang, Z.; Wang, Q.; Hua, N.; Xiao, X.; Cai, S.; Liu, X. Ti_3C_2 MXene Nanosheet/TiO_2 Composites for Efficient Visible Light Photocatalytic Activity. *Ceram. Int.* **2020**, *46*, 25895−25904.
(24) Wang, C.; Cao, M.; Wang, P.; Ao, Y.; Hou, J.; Qian, J. Preparation of Graphene-Carbon Nanotube-TiO_2 Composites with Enhanced Photocatalytic Activity for the Removal of Dye and Cr (VI). *Appl. Catal., A* **2014**, *473*, 83−89.
(25) Woan, K.; Pyrgiotakis, G.; Sigmund, W. Photocatalytic Carbon-Nanotube-TiO_2 Composites. *Adv. Mater.* **2009**, *21*, 2233−2239.
(26) He, Y.; Basnet, P.; Murph, S. E. H.; Zhao, Y. Ag Nanoparticle Embedded TiO_2 Composite Nanorod Arrays Fabricated by Oblique Angle Deposition: Toward Plasmonic Photocatalysis. *ACS Appl. Mater. Interfaces* **2013**, *5*, 11818−11827.
(27) Liu, M.; Wei, S.; Chen, W.; Gao, L.; Li, X.; Mao, L.; Dang, H. Construction of Direct Z-Scheme g-C_3N_4/TiO_2 Nanorod Composites for Promoting Photocatalytic Activity. *J. Chin. Chem. Soc.* **2020**, *67*, 246−252.
(28) Okazaki, M.; Wang, Y.; Yokoi, T.; Maeda, K. Visible-Light-Driven Water Oxidation Using Anatase Titania Modified with First-Row Transition-Metal-Oxide Nanoclusters. *J. Phys. Chem. C* **2019**, *123* (16), 10429−10434.
(29) Maeda, K.; Ishimaki, K.; Okazaki, M.; Kanazawa, T.; Lu, D.; Nozawa, S.; Kato, H.; Kakihana, M. Cobalt Oxide Nanoclusters on Rutile Titania as Bifunctional Units for Water Oxidation Catalysis and Visible Light Absorption: Understanding the Structure−Activity Relationship. *ACS Appl. Mater. Interfaces* **2017**, *9* (7), 6114−6122.
(30) Irie, H.; Miura, S.; Kamiya, K.; Hashimoto, K. Efficient Visible Light- Sensitive Photocatalysts: Grafting Cu(II) Ions onto TiO_2 and WO_3 Photocatalysts. *Chem. Phys. Lett.* **2008**, *457*, 202−205.
(31) Irie, H.; Shibanuma, T.; Kamiya, K.; Miura, S.; Yokoyama, T.; Hashimoto, K. Characterization of Cr(III)-grafted TiO_2 for Photocatalytic Reaction under Visible Light. *Appl. Catal., B* **2010**, *96*, 142−147.
(32) Kitano, S.; Tanaka, A.; Hashimoto, K.; Kominami, H. Selective Oxidation of Alcohols in Aqueous Suspensions of Rhodium Ion-modified TiO_2 Photocatalyst under Irradiation of Visible Light. *Phys. Chem. Chem. Phys.* **2014**, *16*, 12554−12559.
(33) Tanaka, H.; Uchiyama, T.; Kawakami, N.; Okazaki, M.; Uchimoto, Y.; Maeda, K. Water Oxidation through Interfacial Electron Transfer by Visible Light Using Cobalt-Modified Rutile Titania Thin-Film Photoanode. *ACS Appl. Mater. Interfaces* **2020**, *12* (8), 9219−9225.
(34) Jiang, D.; Chu, Z.; Peng, J.; Luo, J.; Mao, Y.; Yang, P.; Jin, W. One-step Synthesis of Three-dimensional $Co(OH)_2$/rGO Nanoflowers as Enzyme-mimic Sensors for Glucose Detection. *Electrochim. Acta* **2018**, *270*, 147−155.
(35) Li, L.; Qian, H.; Ren, J. CdTe@$Co(OH)_2$ (core−shell) Nanoparticles: Aqueous Synthesis and Characterization. *Chem. Commun.* **2005**, 4083−4085.
(36) Wang, J.; Xie, T.; Deng, Q.; Wang, Y.; Zhua, Q.; Liu, S. Three-dimensional Interconnected $Co(OH)_2$ Nanosheets on Ti Mesh as a Highly Sensitive Electrochemical Sensor for Hydrazine Detection. *New J. Chem.* **2019**, *43*, 3218−3225.
(37) Kalasina, S.; Phattharasupakun, N.; Maihom, T.; Promarak, V.; Sudyoadsuk, T.; Limtrakul, J.; Sawangphruk, M. Novel Hybrid Energy Conversion and Storage Cell with Photovoltaic and Supercapacitor Effects in Ionic Liquid Electrolyte. *Sci. Rep.* **2018**, *8*, No. 12192.
(38) Lee, Y.; Theerthagiri, J.; Min, A.; Moon, C. J.; Choi, M. Y. Dual-laser Pulse-patterned α-$Co(OH)_2$/rGO Heterointerface for Accelerated Water Oxidation and Surface Phase-transition via in-situ Raman Spectroscopy. *EcoMat* **2023**, *5*, No. e12417.
(39) Sahoo, D. P.; Nayak, S.; Reddy, K. H.; Martha, S.; Parida, K. Fabrication of a $Co(OH)_2$/ZnCr LDH "p−n" Heterojunction Photocatalyst with Enhanced Separation of Charge Carriers for Efficient Visible-Light-Driven H_2 and O_2 Evolution. *Inorg. Chem.* **2018**, *57* (7), 3840−3854.
(40) Ida, S.; Kearney, K.; Futagami, T.; Hagiwara, H.; Sakai, T.; Watanabe, M.; Angus Rockett, A.; Ishihara, T. Photoelectrochemical H_2 Evolution Using TiO_2-coated $CaFe_2O_4$ without an External Applied Bias under Visible Light Irradiation at 470 nm Based on Device Modeling. *Sustainable Energy Fuels* **2017**, *1*, 280−287.

https://doi.org/10.1021/acsomega.4c10161
ACS Omega 2025, 10, 3101−3107